

Site-specific conjugation of recognition tags to trastuzumab for peptide nucleic acid-mediated radionuclide HER2 pretargeting

Kristina Westerlund^{a,1}, Anzhelika Vorobyeva^{b,1}, Bogdan Mitran^c, Anna Orlova^c, Vladimir Tolmachev^b, Amelie Eriksson Karlström^{a,*}, Mohamed Altai^b

^a Department of Protein Science, School of Engineering Sciences in Chemistry, Biotechnology and Health, KTH Royal Institute of Technology, Stockholm, Sweden

^b Department of Immunology, Genetics and Pathology, Uppsala University, Uppsala, Sweden

^c Division of Molecular Imaging, Department of Medicinal Chemistry, Uppsala University, Uppsala, Sweden



ARTICLE INFO

Keywords:

Antibody
Peptide nucleic acid
Pretargeting
Photoconjugation
Molecular imaging

ABSTRACT

Pretargeting is a promising strategy to reach high imaging contrast in a shorter time than by targeting with directly radiolabeled monoclonal antibodies (mAbs). One of problems in pretargeting is a site-specific, reproducible and uniform conjugation of recognition tags to mAbs. To solve this issue we propose a photoconjugation to covalently couple a recognition tag to a mAb via a photoactivatable Z domain. The Z-domain, a 58-amino acid protein derived from the IgG-binding B-domain of Staphylococcus aureus protein A, has a well-characterized binding site in the Fc portion of IgG. We tested the feasibility of this approach using pretargeting based on hybridization between peptide nucleic acids (PNAs). We have used photoconjugation to couple trastuzumab with the PNA-based hybridization probe, *HP1*. A complementary [⁵⁷Co]Co-labeled PNA hybridization probe ([⁵⁷Co]Co-*HP2*) was used as the secondary targeting probe. In vitro studies demonstrated that trastuzumab-*ZHP1* bound specifically to human epidermal growth factor receptor 2 (HER2)-expressing cells with nanomolar affinity. The binding of the secondary [⁵⁷Co]Co-*HP2* probe to trastuzumab-PNA-pretreated cells was in the picomolar affinity range. A two-fold increase in SKOV-3 tumor targeting was achieved when [⁵⁷Co]Co-*HP2* (0.7 nmol) was injected 48 h after injection of trastuzumab-*ZHP1* (0.5 nmol) compared with trastuzumab-*ZHP1* alone (0.8 ± 0.2 vs. 0.33 ± 0.06 %ID/g). Tumor accumulation of [⁵⁷Co]Co-*HP2* was significantly reduced by pre-saturation with trastuzumab or when no trastuzumab-*ZHP1* was preinjected. A tumor-to-blood uptake ratio of 1.5 ± 0.3 was achieved resulting in a clear visualization of HER2-expressing xenografts as confirmed by SPECT imaging. In conclusion, the feasibility of stable site-specific coupling of a PNA-based recognition tag to trastuzumab and successful pretargeting has been demonstrated. This approach can hopefully be used for a broad range of mAbs and recognition tags.

1. Introduction

Radionuclide molecular imaging provides a promising non-invasive tool for detection of cancer-associated biomarkers. Imaging companion diagnostics offer essential information for patient stratification and effective use of corresponding therapeutic targeting agents. Monoclonal Antibodies (MAbs) have long been considered useful tools for RadioImmunoDiagnostics (RID) [1–3]. Today over 50 antibodies are approved by the US Food and Drug Administration (FDA), and many more are under development [www.fda.gov/drugs/informationondrugs/approveddrugs]. Many of these approved mAbs

are directed against cancer. Their popularity/wide use is based on their well-studied safety profile and ability to specifically recognize aberrantly expressed receptors on cancer cells with high affinity. However, some functional limitations render this class of targeting agents imperfect for imaging applications [4]. The prolonged residence in blood circulation engenders elevated background, which reduces imaging contrast and sensitivity. Moreover, long waiting times between injections and image acquisition limits the choice of appropriate radioisotopes that can be used for adequate imaging in the given time window.

Appreciable efforts have been directed into developing systems that

* Corresponding author. Department of Protein Science, School of Engineering Sciences in Chemistry, Biotechnology and Health, KTH Royal Institute of Technology, 106 91 Stockholm, Sweden.

E-mail address: ameliek@kth.se (A.E. Karlström).

¹ **Author Contributions:** Kristina Westerlund and Anzhelika Vorobyeva contributed equally to this study.

<https://doi.org/10.1016/j.biomaterials.2019.02.012>

Received 16 November 2018; Received in revised form 1 February 2019; Accepted 12 February 2019

Available online 14 February 2019

0142-9612/© 2019 The Authors. Published by Elsevier Ltd. This is an open access article under the CC BY-NC-ND license (<http://creativecommons.org/licenses/by-nc-nd/4.0/>).

circumvent these limitations. One approach has centered upon bioengineering of smaller immunoglobulin formats, such as minibodies, diabodies, and F(ab)₂ fragments, with improved pharmacokinetic profiles [4,5]. These small immunoglobulin-based targeting vectors demonstrated shorter residence time in circulation but their use was associated with low tumor uptake and elevated renal retention of radioactivity.

Engineered Scaffold Proteins (ESPs) have also proven to be promising candidates for targeting applications [6]. The most studied examples of ESPs are Affibody molecules. A number of affibody molecules binding with high affinity to several cancer-associated molecular targets such as, HER2, EGFR, HER3, IGF-1R, PDGFR β and CAIX have been developed. However the number of these target-specific affibody molecules remains limited and many others are still in early phases of development. On the other hand, a large number of mAb candidates are currently approved or in late stage development. Protocols for mAb production are well established and products with high homogeneity and antigen specificity to an “endless” number of targets have been generated. Together this makes mAbs attractive vectors for the delivery of diagnostic and therapeutic radionuclides to malignant tissues.

An alternative strategy to overcome the limitations associated with the use of directly radiolabeled mAbs is pretargeting [7–11]. In pretargeting – or multistep targeting – the two components of radionuclide-based targeting, i.e. the targeting vector and the radioactivity, are uncoupled. The mAb recognizing a tumor-specific antigen contains a recognition tag, forming the primary targeting agent. The secondary agent, modified with another recognition tag, carries the radionuclide and is developed to have an optimal biodistribution profile and fast clearance in comparison with the primary agent. The primary and secondary agents are injected separately and selectively assemble in vivo at the tumor site. Several approaches to pretargeting have been investigated. Earlier work included systems based on (strept)avidin-biotin interactions. The abundance of endogenous biotin and immunogenicity of (strept)avidin has diverted the interest from this method. To avoid cross-reactivity with biological molecules, several groups worked on developing systems based on highly selective reactions between the functional groups of injected components. Most prominent examples include hybridization of complementary nucleic acid analogues, bispecific antibody-hapten interaction and the bioorthogonal inverse electron demand Diels-Alder click reaction. We refer the reader to two review articles for more detailed information about the aforementioned methods [10,11].

A promising approach for pretargeting involves the use of nucleic acid hybridization. Due to their rapid degradation by nucleases, the use of DNA or RNA for in vivo pretargeting appeared to be inappropriate and several alternatives to DNAs have been developed [12,13]. The most studied analogues for pretargeting are the phosphorodiamidate morpholino oligomers (MORFs) and peptide nucleic acids (PNAs) [13–15]. We and others have worked with the synthetic DNA-analogue, PNA [16–21]. PNAs possess a pseudopeptide backbone of repeating N-(2-aminoethyl)glycine units connected via amide bonds [16,22–24]. Due to its unique nature, PNAs are not recognized by either nucleases or peptidases. Their peptidic nature renders them easy to produce using solid-phase synthesis [17]. High rate of PNA hybridization ($1.7 \times 10^5 \text{ M}^{-1} \text{ s}^{-1}$) is advantageous for the secondary agent with fast pharmacokinetics in vivo. Additional advantages include robustness to harsh labeling conditions, lack of toxicity and immunogenicity, and the possibility of chemical modifications. Earlier work from the Hnatowich laboratory demonstrated the feasibility of PNA-based pretargeting [16,25]. This group has clearly demonstrated that it was possible to significantly improve accumulation of radioactivity in tumor in a mouse model using PNA-coupled streptavidin and beads and [^{99m}Tc]Tc-cPNA as primary and secondary injectate, respectively. However, this work relied on nonspecific diffusion of PNA-coupled streptavidin and beads into tumors. Later Leonidova et al. demonstrated that it was possible to use PNA-mediated pretargeting to detect aberrantly-expressed EGFR

receptors in mice using the mAb cetuximab [18]. We have recently investigated the feasibility of PNA-mediated pretargeting using the anti-HER2 Z_{HER2:342} affibody molecule as a targeting agent [19,20]. Experimental therapy study in mice bearing HER2-expressing xenografts showed that mice treated using affibody-based PNA-mediated [¹⁷⁷Lu]Lu-pretargeting had twice longer median survival compared to control groups [21]. While the affibody-based pretargeting is a highly promising approach for targeted radionuclide delivery, however, as highlighted in the previous paragraph, only a limited number of affibody molecules were developed for preclinical use. Alternatively, FDA-approved therapeutic mAbs are promising candidates for primary agents in pretargeting due to their well-characterized safety profile in humans, availability and specificity against a wide range of potential cancer-associated targets.

Extensive research is being done into the conjugation of prosthetic groups or payloads to mAbs [26,27]. Strategies based on N-hydroxysuccinimide (NHS) esters for reactions with amines and maleimide-functionalized probes for thiols are commonly used. Because of the random coupling, different numbers of prosthetic groups may be attached to different positions on mAbs after conjugation, thus generating heterogeneous products. Labeling of lysine residues has been shown to result in a highly heterogeneous antibody product with as many as 20 different sites of modification [28], whereas partial reduction of the interchain disulfide bridges as a strategy to obtain accessible cysteine residues for chemoselective labeling results in more well-defined antibody conjugates [29]. We have earlier developed a novel photolabeling technology to site-specifically decorate mAbs [30–32]. The Z-domain (a derivative of domain B of *Staphylococcus aureus* protein A) is known to have a well-characterized binding site in the Fc portion of IgG [33,34]. By introducing a photoactivable linker in the Z-domain, it was possible to form a covalent bond between the Z-domain and the antibody after irradiation with UV light. Site-specific conjugation provides a homogenous product with a defined degree of modification and predictable pharmacokinetics, which is a serious advantage compared to random coupling approaches reported previously, e.g. coupling of PNA using amine-directed isothiocyanate chemistry reported by Leonidova et al. [18].

In this study, we tested the hypothesis that the use of this novel photoconjugation method for site-specific decoration of mAbs with PNA would provide a primary agent, which is suitable for radionuclide pretargeting in a living system. For proof-of-concept, the well-studied FDA-approved therapeutic mAb trastuzumab (Herceptin[®]) was chosen. Trastuzumab is commercially available and shows chemical robustness making it withstand labeling conditions. It possesses high affinity to the clinically relevant tumor biomarker, HER2. A scheme of the site-specific and covalent labeling of trastuzumab with PNA via the Z-domain is outlined in Fig. 1A. A Z-PNA chimera containing a photoactive cross-linker, Z-HP1, was produced using sortase A catalyzed ligation [17]. Z-HP1 was thereafter covalently crosslinked to the Fc region of the antibody using UV irradiation.

As a secondary agent, the complementary PNA probe HP2, conjugated to the versatile DOTA (1,4,7,10-tetraazacyclododecane-1,4,7,10-tetraacetic acid) chelator, was used (hereinafter denoted as DOTA-HP2). We have shown earlier that DOTA permitted labeling of HP2 with several radiometals [19,20]. The cobalt radioisotope [⁵⁷Co]Co (T_{1/2} = 271.8 d) was used as a surrogate for the PET radioisotope [⁵⁵Co]Co (T_{1/2} = 17.53 d) due its long half-life and convenience. DOTA-HP2 labeled with [⁵⁷Co]Co was used both for in vitro characterization and in animal studies (Fig. 1B).

2. Material and methods

The majority of the chemicals employed in the study were purchased from Sigma-Aldrich Sweden AB. All buffers were prepared using high quality Milli-Q water (resistance higher than 18 M Ω cm). Buffers for radiolabeling of HP2 were treated with Chelex 100 resin (Bio-Rad

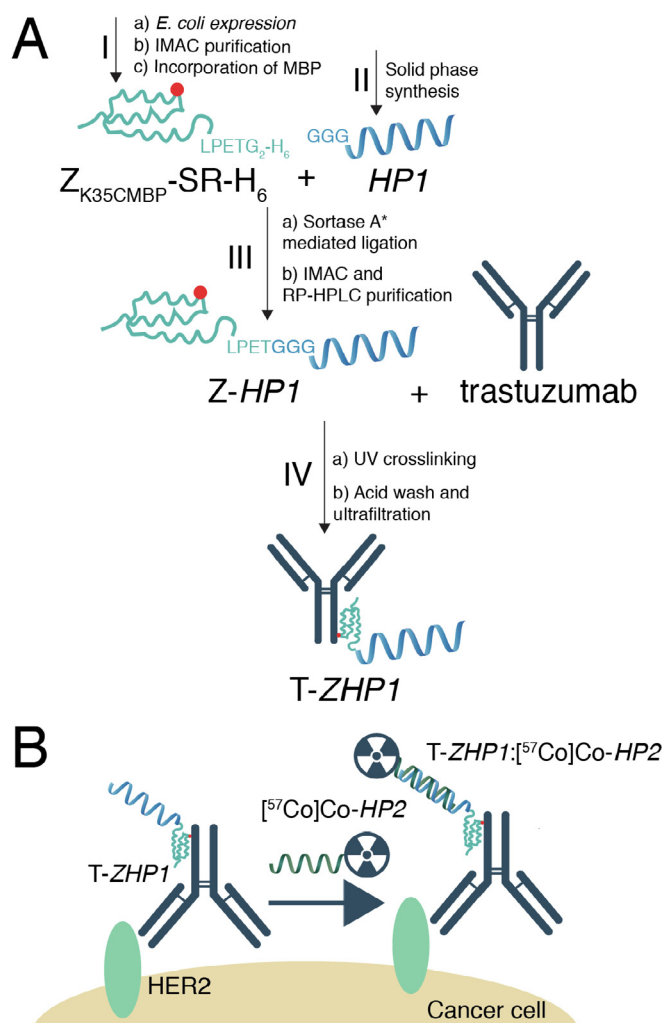


Fig. 1. (A) Schematic illustration of the production of T-ZHP1. (I) A variant of the Z domain with a cysteine at position 35 and a sortase A recognition tag at the C-terminal, Z_{K35C} -SR- H_6 , was expressed in *E. coli* and purified using immobilized metal-affinity chromatography (IMAC). The protein was reduced using dithiothreitol (DTT) and the unique cysteine at position 35 was reacted with the bifunctional photocrosslinker 4-(*N*-maleimido)benzophenone (MBP) to produce $Z_{K35CMBP}$ -SR- H_6 . (II) The PNA-based hybridization probe $HP1$ was assembled using standard Fmoc-protected solid phase synthesis, cleaved off the solid support, and used for enzymatic conjugation to the Z-domain without further purification. (III) $HP1$ was site-specifically coupled to the C-terminal of $Z_{K35CMBP}$ -SR- H_6 using sortase A mediated ligation and the resulting protein-PNA chimera, Z - $HP1$, was purified using IMAC and reversed phase (RP)-HPLC. Trastuzumab, a commercially available hlgG1 full-length antibody, was site-specifically and covalently modified with $HP1$ via the Z domain. (IV) Z - $HP1$ was mixed with trastuzumab and the solution was exposed to UVA irradiation for 2 h. The Z domain has an affinity to bind to the Fc-region of IgGs, and upon UV irradiation the activated benzophenone probe in Z - $HP1$ can covalently cross-link to trastuzumab. As a last step the UV-crosslinked T-ZHP1 was purified using acid wash and a protein concentrator with a molecular weight cut-off of 50 kD to remove any residual unreacted Z - $HP1$. (B) Schematic illustration of the pretargeting strategy presented here. In the first step the primary tumor-targeting agent, T-ZHP1, is injected. Once the primary agent has accumulated at the tumor and cleared from healthy tissue a complementary and radiolabeled PNA strand, $[^{57}\text{Co}]\text{Co-HP2}$, is administered and is allowed to hybridize in vivo with the primary agent.

Laboratories, Richmond, USA) to facilitate the removal of metal contaminants. $[^{57}\text{Co}]$ cobalt chloride was purchased from PerkinElmer Sweden, (Upplands Väsby, Sweden). All radioactive samples were measured in an automated γ -spectrometer with a ~ 7.6 -cm (3-in) NaI

(TI) detector (1480 WIZARD; Wallac Oy). The interaction between modified trastuzumab and HER2 was evaluated using LigandTracer Yellow (Ridgeview AB, Uppsala). LigandTracer Yellow was also used to measure interaction between pretargeting components on cell surface in real time.

2.1. Construction of expression plasmids, and expression and purification of recombinant proteins

A plasmid coding for an affibody molecule with a sortase A recognition tag and a His₆ tag for IMAC purification, pAY430- $Z_{HER2:342}$ -SR- H_6 , has already been constructed by us [17]. The DNA sequence coding for $Z_{HER2:342}$ -part was removed from the plasmid using restriction enzymes *NdeI* and *AccI* (New England Biolabs), and the cut plasmid was purified using agarose-gel electrophoresis and dephosphorylated using alkaline phosphatase (New England Biolabs). The DNA sequence for Z_{WT} was PCR amplified from the plasmid pT7His Z_{WT} , a kind gift from Dr. Feifan Yu (KTH, Sweden) [35], using primers containing *NdeI* and *AccI* restriction sites, double digested with said enzymes, and subcloned into the cut plasmid producing pAY430- Z_{WT} -SR- H_6 . A cysteine (codon underlined in primer) was introduced at position 35 using whole-plasmid mutagenesis with primers 5'-CCAAAGTTTATGCGATGACCCAAAGCAAAG-3' and 5'-ATGAAGCGTTTCGTTGTTC-3'.

The thiol side-chain at position 35 was used for incorporation of the bifunctional photocross-linker maleimido benzophenone (MBP) to be used for UV-radiation driven covalent cross-linking of the Z domain to the heavy chain of trastuzumab.

A small-scale expression-test in *E. coli* revealed that the over-expressed protein is a mixture of Z_{WT} -SR- H_6 with and without the N-terminal initiator methionine. To make sure that the starter methionine is completely excised and a homogenous protein is expressed, an alanine residue was introduced between the initiator methionine and the first amino acid. The alanine was introduced using a round of site-directed whole-plasmid mutagenesis of pAY430- Z_{K35C} -SR- H_6 with a forward primer with a 5'-GCG overhang, producing pAY430-Ala- Z_{K35C} -SR- H_6 . All DNA sequences were verified using sequencing (Microsynth AG). The resulting protein, hereafter called Z_{K35C} -SR- H_6 , has the following sequence: AVDNKFNKEQQNAFYIELHLPNLNNEEQRNAFIQSLCDDPSQS-ANLLAEAKKLNDQAQPKVDGSGSGSLPETGGHHHHHH.

Expression and subsequent IMAC purification of Z_{K35C} -SR- H_6 and the enzyme sortase A^{3*} was done according to previously published protocols for recombinant proteins [17,20], and used without further purification.

2.2. Synthesis and purification of $HP1$ and $HP2$

The hybridization probes $HP1$ (GGGSS-atg ctg gat gta gtc-EK (DOTA)-[AEEA]-E-NH₂) and $HP2$ (DOTA-[AEEA]-SS-gac tac atc cag act-EEY-NH₂), where the amino acids are denoted with upper case letters, PNA monomers are given in lower case letters, and [AEEA] corresponds to [2-(2-aminoethoxy)ethoxy]acetic acid, were synthesized using standard manual solid-phase synthesis using commercially available Fmoc-protected building-blocks as described previously [17,20]. Details of this are presented separately in the Data in Brief communication [36]. The secondary probe $HP2$ was purified using reversed phase HPLC to a final purity of > 95%, freeze-dried from 10 mM ammonium acetate pH 4.5 and stored as dried powder at -20°C .

2.3. Production and purification of Z - $HP1$

Z_{K35C} -SR- H_6 was reduced with 20 mM dithiothreitol (DTT) in 50 mM phosphate buffer, 3 M guanidine hydrochloride (Gdn:HCl), pH 8.0 for 1 h at 37°C . The buffer was changed to PBS pH 6.6 using a PD-10 gel filtration column and reduced Z_{K35C} -SR- H_6 was immediately reacted with 20 X excess of 4-(*N*-maleimido)benzophenone (MBP; Sigma-Aldrich). The reaction, producing $Z_{K35CMBP}$ -SR- H_6 , was left to proceed

over night at room temperature, and unbound MBP was subsequently removed by a PD-10 column equilibrated with sortase A ligation buffer (50 mM Tris base, 150 mM NaCl, 10 mM CaCl₂, pH 7.5).

The primary probe *HP1* was site-specifically coupled to the C-terminal end of Z_{K35CMBP}-SR-H₆ using sortase A mediated ligation as previously described for Z_{HER2:342}-SR-*HP1* in detail in Altai et al. [20]. Briefly, *HP1* (unpurified synthesis product) dissolved in 10% DMSO in water was mixed with 2.5 X excess of Z_{K35CMBP}-SR-H₆ in sortase A ligation buffer and a 5 X excess of Ni²⁺. The reaction was started by addition of 5 μM sortase A^{3*}, left to proceed for 30 min at 37 °C and subsequently stopped by the addition of an equal volume of HisPur Cobalt Resin (Thermo Fisher Scientific), pre-equilibrated in IMAC binding buffer without imidazole (25 mM Na₂HPO₄, 150 mM NaCl, pH 7). After a 30-min incubation at RT the sample/resin slurry was applied to an empty PD-10 column (GE Healthcare), the flow-through was collected, filtrated through a 0.2 μm PVDF membrane and subjected to reversed phase HPLC purification on a Zorbax C18 column (300SB-C18, 9.4 × 250 mm², 5 μm pore size; Agilent) with an elution gradient going from 10 to 45% B over 35 min (A: 0.1% TFA in H₂O; B: 0.1% TFA in CH₃CN) and a flow rate of 3 mL/min. The column temperature was elevated to 70 °C to increase separation. The resulting Z_{K35CMBP}-SR-*HP1* protein-PNA chimera has the following sequence: AVDNKFNKEQQN-AFYEILHLPLNLEEQRNAFIQSLC(MBP)DDPSQSANLLAEAKKLNDAQA-PKVDGSGSGSLPET GGGSS-atg ctg gat gta gtc-EK (DOTA)-[AEEA]-E-NH₂ and is hereinafter denoted as *Z-HP1*. Fractions containing *Z-HP1* were pooled, lyophilized and re-dissolved at a concentration of about 35 μM in 20 mM citrate-phosphate buffer, 150 mM NaCl, pH 6, and stored in 3 mL aliquots wrapped in aluminum foil at −20 °C. The correct molecular weight of *Z-HP1* was verified using mass spectrometry on a MDS SCIEX 4800 MALDI TOF/TOF Analyzer (Applied Biosystems).

2.4. Site-specific cross-linking of *Z-HP1* to trastuzumab

Trastuzumab (Herceptin[®], Roche), a humanized IgG1 HER2-targeting antibody was provided as freeze-dried powder from Apoteket AB, Sweden, dissolved in ultra-pure water to a concentration of 21 μg/μL, and stored at −80 °C in 100 μL aliquots.

In a typical large-scale photoconjugation reaction 14.2 nmol trastuzumab (2.10 mg; 100 μl of 21 μg/μL) was mixed with 71 nmol (5 X excess) of *Z-HP1* (2.17 mL of 32.6 μM) and the volume was adjusted to 10 mL with 20 mM citrate-phosphate buffer, 150 mM NaCl, pH 6. The mixture was transferred to a sterile polystyrene petri dish with a diameter of 92 mm (Sarstedt) and placed on a bed of ice. UV crosslinking was then performed for 120 min in a UVC500 Crosslinker (Amersham) equipped with five 8 V UV-A lights. The UV irradiation was paused every 30 min to change ice and to agitate the solution. After crosslinking the pH of the solution was lowered by the addition of 10 mL of 100 mM glycine-HCl, pH 3. To remove excess of *Z-HP1* not covalently bound to trastuzumab, the solution was centrifuged through an Amicon Ultra-15 centrifugal filter unit with a 50 kDa cut-off (Merck Milipore). The conjugated antibody (hereinafter denoted as T-*ZHP1*) was washed 5 times in the filter unit with 10 mL of 100 mM glycine-HCl, pH 3, and then the pH of the solution was returned to pH 6 by changing the buffer to T-*ZHP1* storage buffer (20 mM citrate-phosphate buffer, 100 mM arginine-HCl, 150 mM NaCl, 100 mg/mL trehalose, 0.05% Tween-20; pH 6) using the same filter unit. Following purification the solution was passed through a 0.2 μm syringe filter and kept at room temperature to prevent protein precipitation.

2.5. Analysis of cross-linking

SDS-PAGE analysis was used to evaluate the conjugation yield for *Z-HP1* conjugated to trastuzumab, to assess the purity of T-*ZHP1* after purification, and to evaluate *HP2* hybridization to T-*ZHP1* under reducing and non-reducing conditions. For reducing gels, trastuzumab, T-*ZHP1* before and after purification, and pre-hybridized T-*ZHP1:HP2*

samples were applied to NuPAGE 4–12% Bis-Tris gels (Thermo Fisher Scientific) and run at 200 V for 40 min at 4 °C under reducing conditions. The gel was stained using GelCode Blue Stain (Thermo Fisher Scientific) according to the manufacturer's instructions and scanned. Gels used for protein band intensity measurements were color adjusted using the Black & White adjustment tool in Adobe Photoshop CC 2015 (Adobe) and their protein band pixel intensities were analyzed using the open source ImageJ software (<http://imagej.nih.gov>). The conjugation yield of T-*ZHP1* in percentage was estimated as the ratio between the band intensities of the conjugated heavy chain to the unconjugated heavy chain x 100. For non-reducing gels, T-*ZHP1* and pre-hybridized T-*ZHP1:HP2*, were mixed with an SDS-PAGE loading buffer without reducing agents and loaded directly onto NuPAGE 4–12% Bis-Tris gels. The non-reducing gels were run at 200 V for approximately 2 h at 4 °C. Non-reducing gels were stained, scanned and protein band intensities were analyzed with ImageJ as described previously for reducing SDS-PAGE gels.

2.6. T-*ZHP1* concentration estimation using SDS-PAGE analysis

SDS-PAGE analysis was used to quantify the T-*ZHP1* concentration after conjugation and purification. Known amounts of trastuzumab (0.32, 0.63, 0.95, 1.26, 1.58 and 1.88 μg) were prepared in 20 mM citrate-phosphate buffer, 150 mM NaCl, pH 6 from a 21 μg/μL trastuzumab stock solution. Trastuzumab standards and T-*ZHP1* samples with unknown concentrations were reduced with 50 mM DTT in 100 mM tris buffer, 7 M urea, 2% SDS, 10% glycerol, 0.001% bromophenol blue; pH 8.0 for 30 min at 37 °C, and alkylated for 15 min in the dark with 200 mM iodoacetamide. Trastuzumab standards and unknown T-*ZHP1* samples (in two different dilutions) were loaded in duplicates on the same 17-well NuPAGE 4–12% Bis-Tris gel. The gel was run, stained and scanned as previously described for reducing SDS-PAGE gels. ImageJ was used to analyze the protein band intensities of trastuzumab and T-*ZHP1*. The intensities of the bands corresponding to the trastuzumab light chain were plotted against the known trastuzumab content in μg. A linear equation was fitted to the data points and the R-squared value was calculated using Excel for Mac 2011 (Microsoft). The linear calibration curve was used to determine the unknown amount of T-*ZHP1* based on the intensity of the unmodified T-*ZHP1* light chain band. The T-*ZHP1* concentration was calculated as the mean of the four samples ± the standard mean deviation. Glycosylated trastuzumab has a molecular mass of 148,400 g/mol (Herceptin Safety Data Sheet, Roche) and a molecular mass of 161,800 g/mol was estimated for T-*ZHP1* (assuming one *Z-HP1* per IgG on average).

2.7. Surface Plasmon resonance based binding analysis

General Surface Plasmon Resonance: All SPR measurements were performed at 25 °C on Biacore systems (GE Healthcare) with CM5 sensor chips. The running buffer, which was also used for analyte dilution, was degassed PBS-T (10 mM Na₂HPO₄, 150 mM NaCl and 0.005% Tween-20; pH 7.4), and the flow rate was set to 50 μL/min in all experiments. Standard NHS/EDC coupling was used to immobilize the ligand covalently to the chip, and following immobilization, the surface was capped with ethanolamine. A reference surface was prepared on each chip by activating the chip surface and then immediately capping it without ligand immobilization. The binding of T-*ZHP1* and trastuzumab to HER2-Fc was studied on a Biacore T200 system, while the binding of *HP2* to T-*ZHP1* and *Z-HP1* was analyzed on a Biacore 3000 system.

For analysis of T-*ZHP1* binding to HER2-Fc, 50 RU (resonance units) of HER2-Fc (Sino Biologicals) was immobilized on the surface of the sensor chip. The T-*ZHP1* storage buffer was exchanged for SPR running buffer using an illustra MicroSpin G-25 column (GE Healthcare), and T-*ZHP1* was injected over the surface at seven different concentrations 6–375 nM (6, 12, 23, 47, 94, 188 and 375 nM). In another experiment,

unconjugated trastuzumab was injected over the same HER2-Fc surface at seven different concentrations 6–385 nM (6, 12, 24, 48, 96, 193 and 385 nM), and the binding was analyzed using the same settings as for T-ZHP1. Association and dissociation times were 300 and 1200 s, respectively. To further study the dissociation part of the binding process 375 nM T-ZHP1 or 385 nM trastuzumab was injected over the HER2-Fc chip surface and the dissociation phase was extended to 5 h. The HER2 surface was regenerated after each run with a 30 s injection of 15 mM HCl and the surface was left to stabilize for 1 h with running buffer before the next injection of analyte.

To study the binding of HP2 to T-ZHP1, approximately 1930 RU of T-ZHP1 was immobilized to the surface of a CM5 sensor chip. To another surface on the same chip 190 RU of Z-HP1 was immobilized, and seven different concentrations between 12 and 750 nM (12, 23, 47, 94, 188, 375 and 750 nM) HP2 were injected over both surfaces. Association and dissociation times were 300 and 1200 s, respectively. The T-ZHP1 and Z-HP1 surfaces were regenerated by a 30 s pulse of 10 mM NaOH followed by a 30 s pulse of 10 mM glycine-HCl; pH 2, and the chip was then left to stabilize with running buffer for an hour before the start of the next experiment.

All SPR experiments were performed in duplicates and the sensorgrams were double referenced by subtracting both the sensorgrams from a blank surface and from an injection of running buffer. Kinetic parameters were estimated from fitting the sensorgrams using a 1:1 Langmuir binding model in BIAevaluation version 4.1, in the case of Biacore 3000, or in Biacore T200 Evaluation software version 2.0 (GE Healthcare).

2.8. Radiolabeling chemistry

T-ZHP1 was radiolabeled with [¹²⁵I] using direct radioiodination method. For this 25 µg (0.16 nmol) T-ZHP1 (62.5 µg/mL PBS) was mixed with [¹²⁵I]NaI (3 µL, 8 MBq). Radioiodination was initiated by the addition of chloramine-T (10 µL, 32 mg/mL in water), and the solution was incubated for 2 min at room temperature. The reaction was quenched by adding sodium metabisulfite (10 µL, 64 mg/mL in water). For comparative purposes, the non-conjugated anti-HER2 mAb trastuzumab (2.1 mg/mL) was radiolabeled with the radioisotope [¹³¹I] by mixing 10 µL (21 µg) of the conjugate with 5 µL [¹³¹I]NaI (6.9 MBq) and then adding Chloramine-T (10 µL, 4 mg/mL in water) to start the reaction. Two minutes later the reaction was quenched by the addition of sodium metabisulfite (10 µL, 8 mg/mL in water). In both cases, a small aliquot (1 µL) of the reaction mixture was analyzed by radio-iTLC, eluted with 80% ethanol. For purification a NAP-5 size exclusion column (GE Healthcare) pre-equilibrated with PBS was used.

For radiolabeling of DOTA-HP2 with [⁵⁷Co]Co, a solution of 25 µg DOTA-HP2 in 70 µL 0.2 M ammonium acetate, pH 5.5, was carefully mixed with 9 µL (9 MBq) [⁵⁷Co]CoCl₂ solution. The mixture was incubated for 40 min at 90 °C. A 1 µL aliquot of the reaction mixture was taken and analyzed by radio-iTLC eluted with 0.2 M citric acid, pH 2.0. No further purification was required as the radiochemical yield of the labeling was > 99%.

2.9. In vitro cell studies

To determine the feasibility and specificity of our pretargeting method in vitro, SKOV-3, BT474 and DU145 cell lines (all from ATCC) with different levels of HER2 expression were used. Petri dishes seeded with ca. 1×10^6 cells/dish of either cell line were divided into four groups (n = 3). All dishes were treated using a standard protocol. First the culture media was aspirated and dishes were washed with 1 mL incomplete serum free medium. After washing, dishes from group 1, 2 and 3 were incubated with 30 nM of the primary targeting agent, T-ZHP1, for 60 min at 4 °C. Thereafter media was discarded and cells were additionally washed with 2×1 mL incomplete serum free media. The radiolabeled secondary probe [⁵⁷Co]Co-DOTA-HP2 (hereafter

designated [⁵⁷Co]Co-HP2) was added to all dishes. Cells were then further incubated with [⁵⁷Co]-HP2 (30 nM) for 60 min at 4 °C. The media were removed and cells were again washed $2 \times$ with 1 mL serum free medium. Cells were then detached by trypsin and the cell-associated radioactivity was measured using automated γ -spectrometer. To evaluate that pretargeting is HER2-mediated, dishes from group 2 were pretreated with a 500-fold molar excess of trastuzumab prior to the addition of T-ZHP1. To confirm that cellular associated radioactivity is a result of hybridization between the PNA probes, dishes from group 3 were pretreated with 30 nM of non-labeled HP2 after incubation with T-ZHP1 and prior the addition of [⁵⁷Co]-HP2. The last set of dishes contained no primary agent T-ZHP1.

A study concerning the cellular processing and internalization of both the primary targeting agent T-ZHP1 labeled with [¹²⁵I] and the cell-bound T-ZHP1:HP2-Co [⁵⁷Co] adduct by HER2-expressing SKOV-3 and BT-474 cells with time was performed according to a method developed and validated by Wållberg and Orlova [37]. To evaluate the processing and internalization of the primary targeting agent, cells were incubated with 3 nM solution of [¹²⁵I]-T-ZHP1 at 4 °C for 60 min. Media were then discarded and cells were further incubated with fresh serum-containing medium at 37 °C. At predetermined time points (1, 2, 4, 8 and 24 h) after incubation, cell-bound and internalized radioactivity was evaluated using an acid wash method. In brief, media was collected (to measure externalized radioactivity) and cells were treated with 4 M urea solution in 0.2 M glycine buffer, pH 2.5, for 5 min on ice. The solution containing detached membrane-bound radioactivity was collected. The cells were then lysed using 1 M NaOH solution to measure the internalized radioactivity at the respective time point. To evaluate the processing and retention of the T-ZHP1:HP2-Co [⁵⁷Co] adduct, cells were preincubated with non-radiolabeled T-ZHP1 for 60 min at 4 °C. Thereafter media was discarded, cells washed with serum free medium and further incubated with 30 nM solution of [⁵⁷Co]Co-HP2 for an additional 60 min (4 °C). Further manipulations were done as described above for [¹²⁵I]-T-ZHP1. The radioactivity of the media, acid wash and base wash samples were then measured using an automated γ -spectrometer.

Binding affinities of [¹²⁵I]-T-ZHP1 to HER2-expressing cells and affinities of [⁵⁷Co]Co-HP2 to T-ZHP1 pretreated cells were measured using LigandTracer-Yellow (Ridgeview Instruments AB, Uppsala) and analyzed by TraceDrawer software (Ridgeview Instruments AB, Uppsala) as described by Tolmachev et al. [38]. Experimental details of this approach are presented separately in the Data in Brief communication [36].

2.10. Animal studies

The animal experiments were planned and performed in accordance with national legislation on protection of laboratory animals. The animal studies were approved by the Local Ethics Committee for Animal Research in Uppsala.

To evaluate the influence of PNA-modified Z-domain on trastuzumab biodistribution, twelve female NMRI mice (average weight 24.9 ± 1.8 g) were randomized to three groups with four mice each. Each group was intravenously injected with a mixture of 300 kBq [¹²⁵I]-T-ZHP1 and 170 kBq [¹³¹I]-T, in 100 µL 2% BSA in PBS. The total amount of injected protein of each was adjusted to 15 µg per animal by adding the non-radiolabeled counterpart. A group of four mice was sacrificed at 6, 24 and 48 h post-injections. The mice were anaesthetized and euthanized by cervical dislocation. Blood was withdrawn by heart puncture. The organ and tissue samples were collected, weighed and measured for radioactivity using an automated gamma-counter along with standards to determine the percentage of injected dose per gram (%ID/g).

For studies involving mice bearing human xenografts, SKOV-3 cells (8×10^6 cells per mouse) were subcutaneously implanted in the right hind leg of female BALB/C nu/nu mice (6–8 weeks old at time of

arrival) 3 weeks before experiment. The average animal weight was 18.8 ± 1.1 g and the average tumor weight was 0.3 ± 0.1 g at the time of experiment. Mice were divided into groups of four. The biodistribution was measured as described above.

The time required by the primary targeting agent to reach an optimal tumor-to-blood ratio was determined using a SPECT/CT imaging study. For this purpose, three BALB/C nu/nu mice bearing SKOV-3 xenografts were injected with [125 I]-T-ZHP1 [30 μ g, 5 MBq, in 100 μ L 2% BSA in PBS]. Mice were then euthanized at 6, 24 and 48 h post injection and whole-body SPECT/CT scans of the injected mice were obtained using a nanoScan SC system (Mediso Medical Imaging Systems).

The specificity of T-ZHP1 binding to HER2-expressing xenografts in vivo was confirmed by injection of [125 I]-T-ZHP1 [80 μ g, 15 kBq, in 100 μ L 2% BSA in PBS] in two groups of mice bearing SKOV-3 xenografts ($n = 8$). However, one group ($n = 4$) was pre-injected (2 h) with a $100 \times$ excess (7.5 mg) of non-labeled trastuzumab to saturate the HER2 receptors. Biodistribution was measured at 72 h post [125 I]-T-ZHP1 injection.

To evaluate in vivo specificity of trastuzumab-based PNA-mediated pretargeting, two groups of BALB/C nu/nu mice bearing SKOV-3 xenografts ($n = 4$) were intravenously injected with 3.5 μ g (0.7 nmol) [57 Co]Co-HP2 [3.5 μ g, 15 kBq, in 100 μ L 2% BSA in PBS containing 4 mg Gelofusine per mouse]. One of the two groups ($n = 4$) was pre-injected with 80 μ g (0.5 nmol) T-ZHP1 [80 μ g, in 100 μ L 2% BSA in PBS] 48 h prior to the injection of [57 Co]Co-HP2. The molar ratio of injected [57 Co]Co-HP2 to T-ZHP1 was 1.4:1. Mice from both groups were sacrificed 24 h post [57 Co]Co-HP2 injection and organs were collected and measured for radioactivity.

To evaluate the influence of the injected dose of the secondary agent [57 Co]Co-HP2 on pretargeting, three groups of mice ($n = 12$) were intravenously injected with T-ZHP1 [80 μ g/0.5 nmol, in 100 μ L 2% BSA in PBS]. Forty-eight hours after injection of the T-ZHP1, mice were injected with 15 kBq [57 Co]Co-HP2 in 100 μ L 2% BSA/PBS containing 4 mg Gelofusine per mouse. The injected mass was adjusted with non-labeled HP2 to 3.5 μ g (0.7 nmol, 1.4:1 HP2:T-ZHP1 molar ratio), 10 μ g (2 nmol, 4:1 HP2:T-ZHP1 molar ratio) or 20 μ g (4 nmol, 8:1 HP2:T-ZHP1 molar ratio). Twenty-four hours after [57 Co]Co-HP2 injection, the animals were sacrificed and the distribution of activity was measured as described earlier.

To confirm that pretargeting is HER2 mediated, an additional group of BALB/C nu/nu mice bearing SKOV-3 xenografts ($n = 4$) was intravenously injected with T-ZHP1 [80 μ g/0.5 nmol in 100 μ L 2% BSA in PBS]. Mice were injected with a $100 \times$ excess (7.5 mg) of trastuzumab, 2 h prior to the injection of T-ZHP1. Forty-eight hours later mice were intravenously injected with 3.5 μ g (0.7 nmol) [57 Co]Co-HP2 [3.5 μ g, 15 kBq, in 100 μ L 2% BSA in PBS containing 4 mg Gelofusine per mouse]. Animals were then sacrificed 24 h post [57 Co]Co-HP2 injection and manipulated as mentioned earlier.

2.11. Imaging

Results from the biodistribution experiments were confirmed using SPECT imaging. Four BALB/C nu/nu mice bearing SKOV-3 xenografts were divided into two groups ($n = 2$). One group of mice were intravenously injected with T-ZHP1 [80 μ g in 100 μ L 2% BSA in PBS]. Forty-eight hours later all four mice were intravenously injected with 3.5 μ g (0.7 nmol) [57 Co]Co-HP2 [1.4:1 HP2:T-ZHP1 molar ratio, 2.7 MBq, in 100 μ L 2% BSA/PBS containing 4 mg Gelofusine per mouse]. Mice were then euthanized 24 h post [57 Co]Co-HP2 injection and whole-body SPECT/CT scans of the injected mice were obtained using a nanoScan SC system (Mediso Medical Imaging Systems).

3. Results and discussion

3.1. Production, purification and site-specific cross-linking of Z-HP1 to trastuzumab

Here we describe the site-specific labeling of trastuzumab with a PNA-based hybridization probe, HP1, via the Z domain (Fig. 1A). The Z domain has previously been used to modify commercially available full-length IgGs with, for example, biotin, fluorophores and azide moieties [30,32,39]. Earlier studies have identified position 35 in Z-domain as the best position to introduce an unnatural amino acid with a benzoylphenyl side-chain for efficient UV crosslinking to hlgG1 [40]. Our Z-variant was bacterially expressed with a cysteine at position 35 and a sortase A recognition tag, LPETG, at the C-terminus for downstream conjugation with 4-(N-maleimido)benzophenone (MBP) via maleimide chemistry and enzymatic conjugation to HP1, respectively. We have previously used the enzyme sortase A for efficient and site-specific conjugation of a PNA-based hybridization probe, HP1, to an anti-HER2 antibody molecule [17,20] and the same enzymatic strategy was used here. The purity of the Z-HP1 construct was over 90% before the UV-crosslinking to trastuzumab according to HPLC-MS analysis (theoretical MW 13428.2 Da, experimental MW 13428.7 Da). Analysis of the UV crosslinking efficiency shows that 50% of heavy chains in trastuzumab were conjugated with Z-HP1 (Fig. 2A, lane 3) or, on average, one Z-HP1 per full-length antibody. A further characterization of IgG populations under non-reducing conditions (Fig. 2B, lane 1) showed that 47% of all intact antibodies were covalently conjugated with one Z-HP1 molecule, while 22% were doubly conjugated. Taken together, this means that approximately 69% of all IgGs were covalently labeled with at least one HP1 probe. Pre-hybridization with HP2 produced small but distinct shifts in the electrophoretic mobility of heavy chains (Fig. 2A, lane 4)

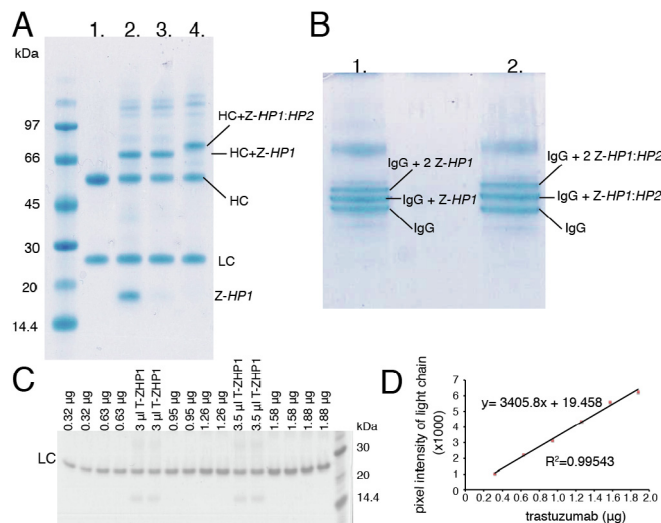


Fig. 2. (A) Reducing SDS-PAGE gel of the cross-linking reaction. Lane 1: unconjugated trastuzumab, lane 2: un-purified T-ZHP1 after photoconjugation, lane 3: purified T-ZHP1, and lane 4: T-ZHP1 incubated with an excess of HP2. Analyses of the Z-HP1 bands before and after purification indicate that less than 14% of the free unconjugated Z-HP1 is left after purification. (B) Non-reducing SDS-PAGE gel. Lane 1: T-ZHP1, and lane 2: T-ZHP1 incubated with an excess of HP2. (C) Typical reducing SDS-PAGE gel used to quantify T-ZHP1 after purification. Six different standard amounts of trastuzumab (0.32–1.88 μ g) were run on the gel together with two dilutions of a T-ZHP1 sample of unknown concentration. All samples were run in duplicates. Light chain (LC) pixel intensities for all samples were analyzed using ImageJ software and the average pixel intensities of the trastuzumab standards were plotted against the protein content in (D). A linear equation was fitted to the data points and this standard curve was then used to determine the concentration (0.359 ± 0.008 μ g/ μ L) of the T-ZHP1 sample.

and full length IgGs (Fig. 2B, lane 2) conjugated to Z-HP1 in both reducing and non-reducing SDS-PAGE gels. The calculated conjugation efficiencies presented here are in good agreement with results previously published [32,40]. After purification by acid wash and filtration, performed in order to separate noncovalently bound Z-HP1 from the antibody, the T-ZHP1 concentration was estimated using reducing SDS-PAGE with a trastuzumab standard curve (Fig. 2C and D).

These results show that it is possible to site-specifically functionalize a commercially available mAb with PNA, using a single UV conjugation step. Importantly, the generated product has a defined stoichiometry, in contrast to random labeling of lysine or cysteine residues. In theory, this means that it would be possible to convert any therapeutic antibody into its companion diagnostic agent, an important tool to measure the therapeutic target expression during drug development and clinical treatment. The strategy does not require further engineering of the antibody, in contrast to e.g. the Thiomab technology, where site-selective labeling is achieved by introduction of an unpaired cysteine residue [41], or sortase A-mediated conjugation, relying on the addition of a sortase A recognition motif to the antibody polypeptide chains [42]. Preparation of the modified Z domain for the photolabeling requires a few synthetic steps, but the strategy is versatile as the same reagent can be used for labeling of a panel of different antibodies. A tremendous amount of effort has gone into development of companion diagnostic agents based on radiolabeled antibodies [43]. However, inherent limitations of antibodies, such as long half-life (several days), have complicated their development as diagnostic agents [44]. We believe that the developed novel site-specific conjugation method reported in this study in combination with pretargeting represents a suitable approach to address these limitations.

3.2. Estimation of the dissociation constants at equilibrium, K_D

Researchers at Genentech have previously estimated a sub-nanomolar equilibrium dissociation constant, K_D , (0.5 ± 0.1 nM) for the interaction between Herceptin/trastuzumab and HER2-ECD using surface plasma resonance (SPR) [45]. In Fig. 3A–C we used SPR to evaluate if T-ZHP1 retains a high affinity to the HER2 receptor. The association constant for the interaction, k_a , was estimated to $2 \times 10^5 \text{ M}^{-1} \text{ s}^{-1}$, which is in excellent agreement with $2 \times 10^5 \text{ M}^{-1} \text{ s}^{-1}$ measured for the interaction between trastuzumab and HER2 on the same chip. These values are also in agreement with the association constant previously reported for Herceptin ($k_a = 7.1 \pm 0.5 \times 10^5 \text{ M}^{-1} \text{ s}^{-1}$) [45]. Dissociation rate constants (k_d s) for the interactions were too slow to be determined from a 20-min dissociation phase in Fig. 3A and B, and the dissociation phase was extended to 5 h for 375 nM T-ZHP1 and 385 nM trastuzumab in Fig. 3C. A k_d value of $2 \times 10^{-5} \text{ s}^{-1}$ was observed for the interaction between T-ZHP1 and HER2-Fc, but this value is close to the limit of accurate determination by the SPR instrument and should only be regarded as an approximation. The dissociation of trastuzumab/HER2 complex was deemed too slow to be determined using the Biacore T200 system ($k_d \leq 10^{-5} \text{ s}^{-1}$), and no K_D could thus be determined for trastuzumab. A K_D of 0.1 nM was estimated for the T-ZHP1/HER2-Fc interaction, which indicates that T-ZHP1 retains a sub-nanomolar affinity for the HER2 receptor.

Fig. 3D and E shows HP2 binding to immobilized T-ZHP1 and to Z-HP1, respectively. The association rate constants were very similar for HP2 hybridizing to T-ZHP1 ($1.1 \times 10^5 \text{ M}^{-1} \text{ s}^{-1}$) and Z-HP1 ($1.8 \times 10^5 \text{ M}^{-1} \text{ s}^{-1}$), and both are in excellent agreement with the k_a value ($1.7 \times 10^5 \text{ M}^{-1} \text{ s}^{-1}$) determined previously by us for HP2 binding to $Z_{\text{HER2:342}}\text{-SR-HP1}$ [17]. The dissociation rate constants were in both cases too slow to be determined from the sensorgrams in Fig. 3D and E. HP2 binding to $Z_{\text{HER2:342}}\text{-SR-HP1}$ has previously been shown to have to have an extremely slow off-rate and even a 17 h long dissociation phase resulted in < 5% dissociation of the formed complex [17].

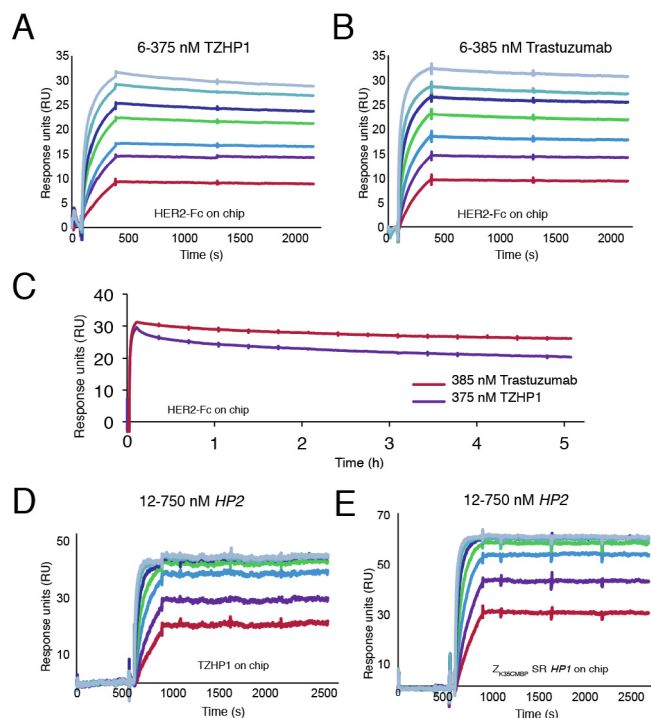


Fig. 3. Representative SPR sensorgrams of (A) T-ZHP1 and (B) trastuzumab binding to immobilized HER2-Fc. (C) Both trastuzumab and T-ZHP1 experience a slow dissociation from the HER2-receptor with rate constants below (trastuzumab) or close to (T-ZHP1) the limit of accurate detection for the instrument. Biacore sensorgrams of HP2 injected over (D) T-ZHP1 and (E) Z-HP1. HP2 was injected over both surfaces at seven different concentrations 12–750 nM. All experiments in A–E were done in duplicates.

3.3. Radiolabeling chemistry

Labeling of Z-HP1-conjugated trastuzumab (T-ZHP1) with [^{125}I]I, trastuzumab with [^{131}I]I and the secondary agent HP2 with [^{57}Co]Co was successful. The radiochemical yields were $67.5 \pm 3.5\%$ for [^{125}I]I-T-ZHP1, $95.8 \pm 2\%$ for [^{131}I]I-T and $99.2 \pm 0.98\%$ for [^{57}Co]Co-HP2. Size exclusion chromatography purification of [^{125}I]I-T-ZHP1 provided a radiochemical purity of more than 95%. Both [^{131}I]I-T and [^{57}Co]Co-HP2 required no further purifications. It is worth mentioning that the use of DOTA would enable labeling HP2 with a broad range of radionuclides [46]. Keeping in mind that HP2 demonstrates short half-life in vivo (~ 13 min, as previously reported by us [21]), this means that it would be possible to utilize promising short-lived PET radioisotopes like [^{68}Ga]Ga and [^{64}Cu]Cu for antibody-based pretargeting imaging. This is conceptually innovative as otherwise the half-life of these imaging radionuclides is too short to prove effective under the slow pharmacokinetic conditions characterizing directly labeled antibodies.

3.4. In vitro cell studies

[^{125}I]I-T-ZHP1 retained the capacity to bind to HER2-expressing living cells with high affinity ($K_D = 1 \pm 0.4$ and 0.5 ± 0.3 nM in SKOV-3 and BT474, respectively) see Fig. 1 in the Data in Brief communication [36] and Table 1. The dissociation constant at equilibrium K_D of the parental mAb (trastuzumab) was 1.1 ± 0.8 and 1.9 ± 1.1 nM in SKOV-3 and BT474, respectively. These results again confirm that site-specific functionalization of the Fc-region of trastuzumab with Z-HP1 has no profound effect on the binding properties.

Results from the in vitro specificity experiment clearly demonstrated the feasibility and specificity of our pretargeting method (Fig. 4). Binding of [^{57}Co]Co-HP2 to three different HER2-expressing cell lines pretreated with the primary targeting agent T-ZHP1 was

Table 1

Equilibrium dissociation constants (K_D) for binding of radiolabeled T-ZHP1 and trastuzumab to SKOV-3 and BT474 cells measured using LigandTracer.

	K_D (nM)	
	SKOV-3	BT474
Trastuzumab	0.98 ± 0.36	0.50 ± 0.32
T-ZHP1	1.07 ± 0.79	1.84 ± 1.16

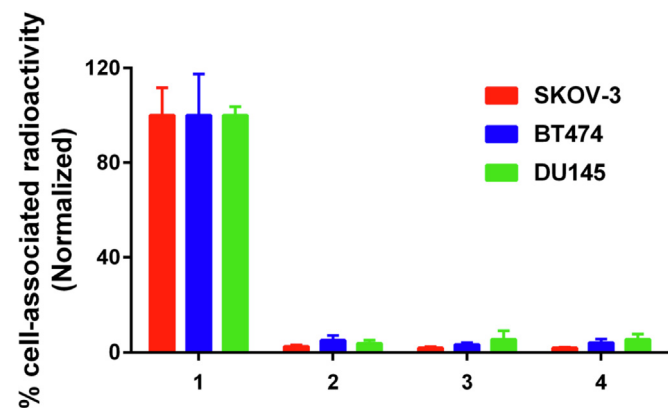


Fig. 4. Binding of [^{57}Co]Co-HP2 to SKOV-3 (white), BT474 (black) and DU145 (grey). Cells of **group 1** were first incubated with 30 nM T-ZHP1 for 1 h at 37°C prior to the addition of 30 nM [^{57}Co]Co-HP2. In **group 2** a 500-fold molar excess of trastuzumab was added to block HER2-receptors prior to the addition of the primary targeting agent T-ZHP1. To determine specificity of HP1-HP2 hybridization, cells in **group 3** were incubated with an excess of unlabeled HP2 after incubation with T-ZHP1 and prior to the addition of [^{57}Co]Co-HP2. [^{57}Co]Co-HP2 was directly added to cells in **group 4** without pretargeting. Cell-associated activity is normalized to the average in the **group 1**. Data are presented as an average and standard deviation ($n = 3$).

significantly higher compared to all other control groups. Binding was significantly reduced when no primary T-ZHP1 was added, which confirms a PNA-PNA hybridization-mediated cellular uptake of radioactivity (Fig. 4). Cellular binding of [^{57}Co]Co-HP2 was also reduced when cells were presaturated with trastuzumab prior to the addition of the primary agent T-ZHP1; this result clearly indicates that availability of HER2 receptors is a precondition for successful pretargeting.

An important precondition for efficient pretargeting is the availability of the primary agent on the cell surface. Cellular processing studies of [^{125}I]I-T-ZHP1 demonstrated that after 24 h, 21 ± 1% (SKOV-3) and 17 ± 1% (BT474) of the added targeting vector was membrane bound (Fig. 5). These results indicate that the primary agent is available on the cell surface for the reaction with the secondary agent even 24 h after the injection of T-ZHP1. It is apparent that shortening the time interval between the administrations of the pretargeting components would result in more efficient pretargeting due to better

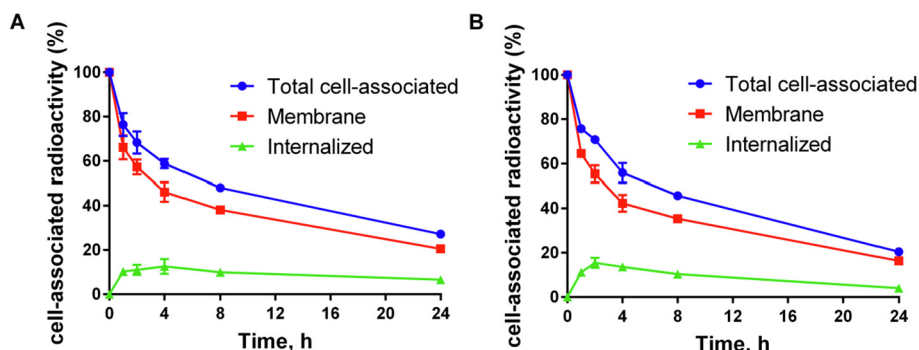


Fig. 5. In vitro cellular processing of [^{125}I]I-T-ZHP1 by SKOV-3 (A) and BT474 (B) cell lines. Cells were incubated with 3 nM [^{125}I]I-T-ZHP1 for 1 h at 37°C. An acid wash was used to determine membrane-bound radioactivity. Cells were lysed using 1M NaOH to determine internalized radioactivity. Data are presented as a mean value and standard deviation for three cell culture dishes. Error bars might be smaller than the symbols and are therefore not seen.

Table 2

Equilibrium dissociation constants (K_D) for the interaction of [^{57}Co]Co-HP2 with SKOV-3 and BT474 cells pretreated with 30 nM T-ZHP1 for 1 h estimated using LigandTracer.

	K_D (pM)	
	K_{D1}	K_{D2} (nM)
SKOV-3	39 ± 25	44 ± 34
BT474	67.6 ± 0.54	12.3 ± 5.7

availability of T-ZHP1 bound to the membrane. Results from the cellular processing experiment support this assumption and there is a higher proportion of T-ZHP1 bound to cell membrane at earlier time points (Fig. 5).

Measurements of binding kinetics of [^{57}Co]Co-HP2 to HER2-expressing cells pretreated with 30 nM T-ZHP1 using LigandTracer are shown in Fig. 2 in the Data in Brief communication [36]. Fitting of the binding kinetics curves revealed that the interaction is determined by two affinities; one in pM range K_{D1} (39 ± 25 and 67.6 ± 0.54, for SKOV-3 and BT474, respectively) and the other in nM range K_{D2} (44 ± 34 and 12.3 ± 5.7, for SKOV-3 and BT474 respectively), see Table 2. We have observed a similar phenomenon earlier when developing an affibody-dependent PNA-mediated pretargeting system [19]. We believe that the binding kinetics between the radiolabeled secondary HP2 and cell-bound T-ZHP1 targeting agents in living cells is not determined only by the interaction between the two components on the cell surface. The interplay of several interactions may also be involved. These may include interaction of T-ZHP1 with HER2, interaction of radiolabeled HP2 with cell-bound T-ZHP1 and the interaction of the T-ZHP1:HP2-Co [^{57}Co] adduct with HER2 receptors. Björkelund and co-workers have also shown earlier that the interaction between ligands and HER receptors may be altered by the degree of homo- and heterodimerization of these receptors [47]. This finding reveals an extra degree of complexity to the ligand-cell interaction puzzle.

Data concerning the cellular processing and internalization of the T-ZHP1:HP2-Co [^{57}Co] adduct are presented in Fig. 6A and B. The radioactivity was efficiently retained by HER2-expressing cells. High amounts of cell-associated radioactivity were retained after 24 h incubation at 37°C (67 ± 0.1% for SKOV-3 and 70 ± 1.8% for BT474 cells). Most of the retained radioactivity was membrane-bound in SKOV-3 cells after 24 h. However, for BT474 cells there was a more equal distribution of retained radioactivity between the membrane and intracellular fractions. High cellular retention after internalization is of utter importance to elevate the tumor-associated radioactivity.

3.5. Animal studies and imaging

Biodistribution data showed that modification of Z-HP1 to the Fc region of trastuzumab by site-specific conjugation of Z-HP1 to the Fc region of trastuzumab resulted in a more rapid clearance of the targeting agent T-ZHP1 from blood and other body compartments compared to the non-modified antibody (Fig. 7). One possible explanation for this difference may stem

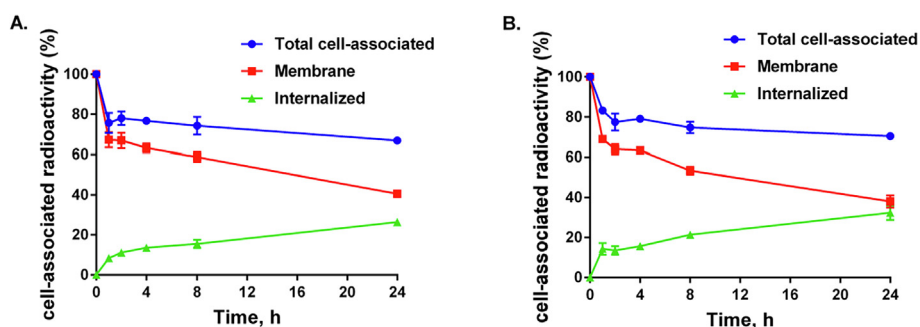


Fig. 6. In vitro cellular processing of ^{57}Co -HP2 by SKOV-3 (A) and BT474 (B) cells pretreated with 30 nM T-ZHP1 for 60 min at 4°C. Cells were then incubated with 30 nM solution of [^{57}Co]Co-HP2 for 1 h at 37°C. Incubation media was discarded and at predetermined time points an acid wash method (described above) was used to discriminate between membrane-bound and internalized radioactivity. Data are presented as a mean value and standard deviation for three cell culture dishes. Error bars might be smaller than the symbols and are therefore not seen.

from the difference in interaction with the neonatal Fc receptor (FcRn) that regulates the serum half-life of IgGs and protects them from degradation. It was shown earlier that mutations of the FcRn binding site in the Fc domain resulted in an enhanced elimination and abbreviated serum half-life of IgGs [48,49]. Induced rapid clearance of T-ZHP1 from blood is advantageous in pretargeting applications, as this would reduce interception of the radiolabeled secondary targeting agent by the residual primary agent.

SPECT images of the in vivo distribution of the primary agent demonstrated that the optimal tumor-to-background ratio of radioactivity was achieved 48 h after [^{125}I]I-T-ZHP1 injection in mice bearing SKOV-3 xenografts (Fig. 8). Moreover, the HER2-blocking experiment demonstrated that the binding of [^{125}I]I-T-ZHP1 to HER2-expressing SKOV-3 xenografts in vivo is specific and mediated by HER2 (Fig. 9).

Comparison of [^{57}Co]Co-HP2 biodistribution with and without preinjection of T-ZHP1 demonstrated that the tumor uptake of [^{57}Co]Co-HP2 is dependent on the presence of HP1 (Fig. 10A). Preinjection of T-ZHP1 resulted in a significantly higher uptake of [^{57}Co]Co-HP2 in the tumor (0.8 ± 0.2 vs. $0.03 \pm 0.01\%$ ID/g) (Fig. 10A). We also observed significantly higher retention of [^{57}Co]Co-HP2 in the blood and all normal organs and tissues. This, presumably, reflects interception of injected secondary [^{57}Co]Co-HP2 by residual non-cleared T-ZHP1 in the blood. Previous studies involving the development of PNA-mediated pretargeting systems have demonstrated similar results [16,18]. Increasing the time between the two injections or the introduction of a clearing agent may reduce blood-borne activity and improve imaging contrast, as well as provide better dosimetry in pretargeted therapy [21,50,51].

Administration of trastuzumab prior to the injection of the primary targeting agent T-ZHP1 resulted in more than 2-fold decrease of [^{57}Co]Co-HP2 localization in HER2-expressing xenografts (0.8 ± 0.2 vs. 0.3 ± 0.05 %ID/g, respectively) (Fig. 10A). This blocking experiment clearly indicates that our pretargeting approach is dependent on specific binding of the primary targeting agent T-ZHP1 to HER2-receptors, i.e. HER2-mediated.

We hypothesized that increasing the injected mass of HP2 may help to saturate residual T-ZHP1 in the blood and increase the amount of radiolabeled effector to be delivered to the tumors (Fig. 10B). As expected, increasing the HP2-to-T-ZHP1 injected mass ratio from 1.4:1 ($3.5 \mu\text{g}/0.7 \text{ nmol}:80 \mu\text{g}/0.5 \text{ nmol}$) to 4:1 ($10 \mu\text{g}/2 \text{ nmol}:80 \mu\text{g}/0.5 \text{ nmol}$) and 8:1 ($20 \mu\text{g}/4 \text{ nmol}:80 \mu\text{g}/0.5 \text{ nmol}$) decreased the retention of radioactivity in the blood significantly. However, the tumor uptake of [^{57}Co]Co-HP2 was also significantly ($P < 0.05$) reduced (0.8 ± 0.2 vs. 0.4 ± 0.1 and 0.18 ± 0.03 %ID/g, for 3.5, 10 and 20 μg injected [^{57}Co]Co-HP2, respectively). We have observed a similar effect when developing non-immunoglobulin based pretargeting systems [19,52]. These data indicate that the optimal pretargeting and the highest tumor-to-blood ratios were achieved at the molar ratio of 1.4:1 of HP2 to T-ZHP1. Importantly, the optimal dose finding experiment also revealed a saturable character of HP2 accumulation in T-ZHP1-treated xenografts. This provides additional evidence that localization of [^{57}Co]Co-HP2 in the tumor is primarily mediated by interaction of

HP2 with HP1.

Pretargeting using [^{125}I]I-T-ZHP1 and [^{57}Co]Co-HP2 at 24 h post-injection provided an increase in radioactivity delivered to tumors compared to direct targeting using trastuzumab at 72 h (0.8 ± 0.2 vs. 0.33 ± 0.06 %ID/g). Combined with a decrease in the blood-borne radioactivity (0.5 ± 0.06 vs. 0.9 ± 0.2 %ID/g), pretargeting significantly improved tumor-to-blood ratios from 0.4 ± 0.03 to 1.5 ± 0.3 , which would translate to improved imaging contrast and sensitivity (Fig. 11). The full data from Fig. 11 are presented separately in Tables 1 and 2 in the Data in Brief communication [36].

We have earlier shown that for affibody-mediated pretargeting it was possible to inject HP2 as early as 4 h post affibody-HP1 injection [19]. Rapid clearance of affibody-HP1 (as well as slow internalization) enabled this early injection of radiolabeled-HP2, which allowed for high radiation doses to be delivered to tumors through increased PNA-PNA hybridization at the cell surface [19]. Therefore, to further maximize the benefits of using PNA-mediated pretargeting in combination with mAbs we are currently developing a clearing agent designed to accelerate the removal of residual mAb-PNA conjugate from circulation. We envision that this would enable injection of radiolabeled HP2 at an earlier time point when more of T-ZHP1 is still located at the tumor cell surface.

Earlier, Leonidova et al. reported pretargeting in mice bearing EGFR-expressing A431 xenografts [18]. Mice were injected with a PNA-cetuximab conjugate 24 h prior to the administration of [$^{99\text{m}}\text{Tc}$]Tc-radiolabeled complementary PNA. Twenty-four hours post injection of [$^{99\text{m}}\text{Tc}$]Tc-PNA the tumor-to-blood radioactivity uptake ratio reached a level of 0.48 ± 0.09 . Although a direct comparison may not be possible due to differences in targeted receptor (EGFR vs. HER2), composition of PNAs, method and degree of mAb conjugation, used radionuclides, time of injection and administered doses, it would still be reasonable to conclude that our currently investigated system provided adequate tumor-to-non tumor uptake ratios, a prerequisite for high contrast imaging.

Moreover, tumor to non-targeted organ uptake ratios have also improved significantly using pretargeting. Of importance is the 5-fold increase in tumor-to-bone uptake ratio compared to direct targeting. This may be of great advantage for imaging of some types of cancer, e.g. prostate cancer with distant metastases in bone or bone marrow.

On the basis of these promising results, proof-of-principle SPECT imaging using pretargeting was conducted in nude mice bearing HER2-expressing SKOV-3 xenografts (Fig. 12). Imaging confirmed the results of the biodistribution experiments. Using pretargeting it was possible to visualize HER2-expressing SKOV-3 xenografts 24 h after injection of [^{57}Co]Co-HP2. In agreement with the ex vivo experiments, moderate to low accumulation of radioactivity was observed in blood, liver and kidneys. The tumor uptake exceeded the uptake in any other tissue except the kidneys. No accumulation of radioactivity was observed in the tumor in the absence of T-ZHP1. Cobalt-57 was used for this first proof-of-principle study due to its long half-life and availability; the substitution of [^{57}Co]Co with the long-lived positron emitter [^{55}Co]Co ($T_{1/2}$ 17.5 h) for PET imaging is envisioned [53]. We believe that

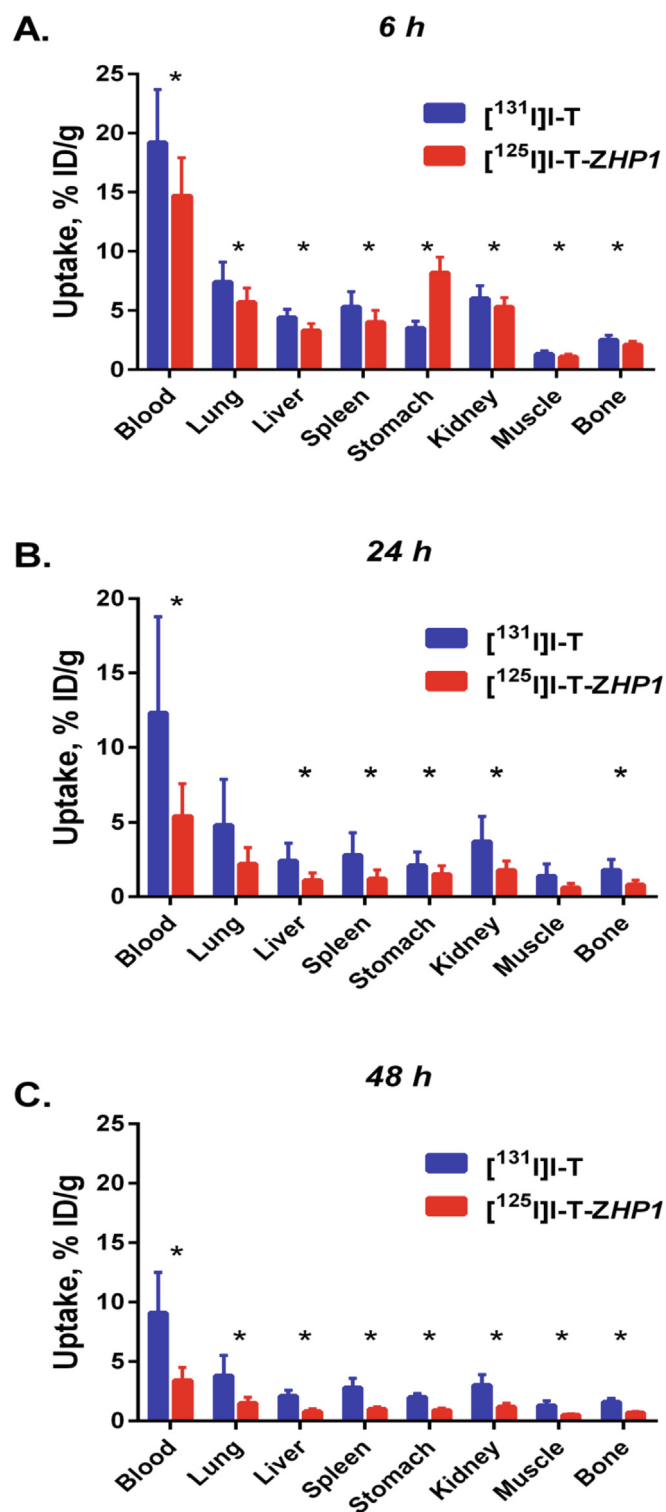


Fig. 7. Comparative biodistribution of [¹²⁵I]I-T-ZHP1 and [¹³¹I]I-T in NMRI normal mice at 6 (A), 24 (B) and 48 (C) h p.i. The uptake in different organs is expressed as %ID/g and presented as an average value from four animals ± standard deviation. Asterisks (*) indicates significant difference (p < 0.05 in paired student's t-test) between [¹²⁵I]I-T-ZHP1 and [¹³¹I]I-T.

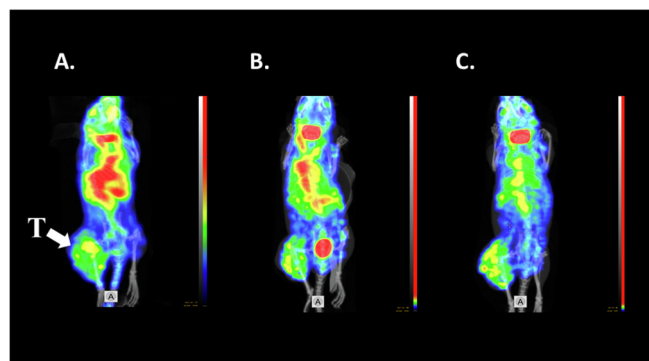


Fig. 8. SPECT images of BALB/C nu/nu mice bearing SKOV-3 xenografts injected with [¹²⁵I]I-T-ZHP1. Mice were euthanized at 6 (A), 24 (B) and 48 (C) h p. i. and whole body scans were obtained using a nanoScan SC system. (T) Tumor.

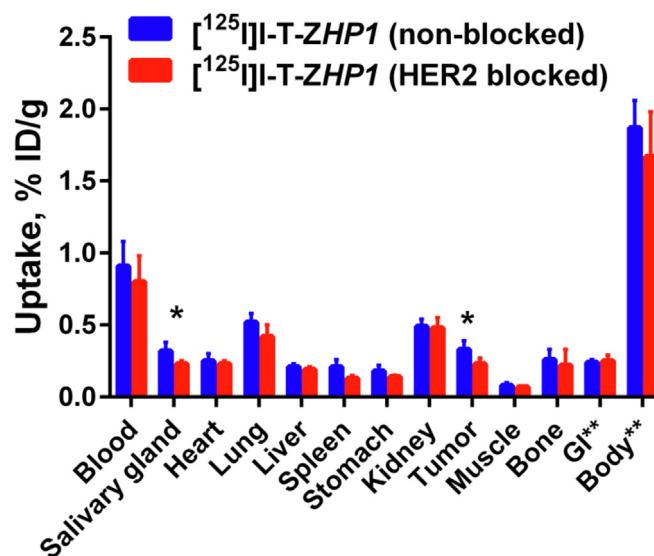


Fig. 9. In vivo targeting demonstrating the HER2 specificity of [¹²⁵I]I-TZHP1 at 72 h p.i. without (black) and with (white) preinjection of 7.5 mg trastuzumab. The uptake in different organs is expressed as %ID/g and presented as an average value from four animals ± standard deviation. Asterisks (*) indicates significant difference (p < 0.05 in paired student's t-test) in organ uptake. **Uptake in gastrointestinal tract (GI tract) and remaining body is presented as %ID per whole sample.

combining pretargeting and PET would have a profound outcome on imaging sensitivity.

4. Conclusion

The feasibility of our antibody-based PNA-mediated pretargeting system was demonstrated both in vitro and in vivo using the therapeutic mAb, trastuzumab. Trastuzumab was site-specifically functionalized with the hybridization probe, HP1, using a novel in-house developed conjugation method. Trastuzumab retained its binding capacity after the conjugation to Z-HP1. Using pretargeting it was possible to significantly increase accumulation of radioactivity in HER2-expressing tumors while reducing the uptake in non-targeted organs compared to direct targeting. SPECT imaging confirmed biodistribution results. The presented method is versatile in its nature as it could be applied for modification of mAbs targeting different biomarkers other than HER2. PET imaging using mAbs in combination with short-lived PET-radioisotopes appears to be promising with the presented approach. Additionally, the results from the current study indicate that further

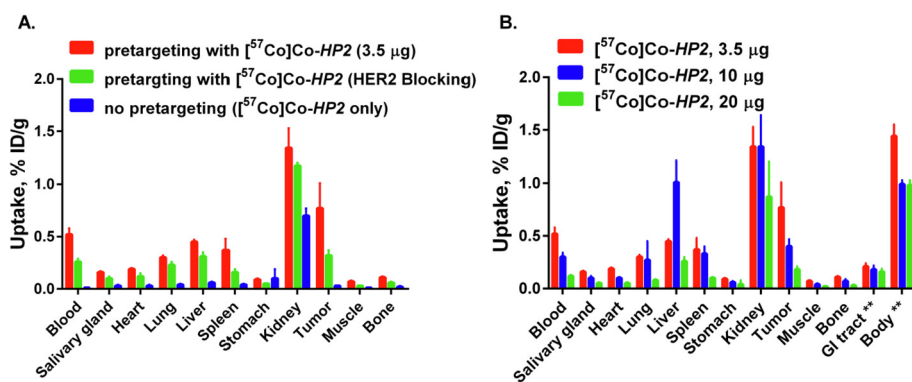


Fig. 10. (A) In vivo biodistribution of 3.5 µg $[^{57}\text{Co}]\text{Co-HP2}$ 24 h p.i. in mice bearing SKOV-3 xenografts when mice were intravenously pre-injected with 80 µg T-ZHP1 (white), mice were injected with 7.5 mg trastuzumab prior to pretargeting protocol (black) and without pre-injection of T-ZHP1 (grey). (B) Influence of injected mass of $[^{57}\text{Co}]\text{Co-HP2}$ on pretargeting. Mice were injected with 80 µg T-ZHP1, 48 h prior to the injection of either 3.5, 10 or 20 µg $[^{57}\text{Co}]\text{Co-HP2}$. Mice were euthanized 24 h after $[^{57}\text{Co}]\text{Co-HP2}$ injection. Uptake is expressed as % ID/g and presented as an average of four mice \pm SD. **Uptake in gastrointestinal tract (GI tract) and remaining body is presented as %ID per whole sample.

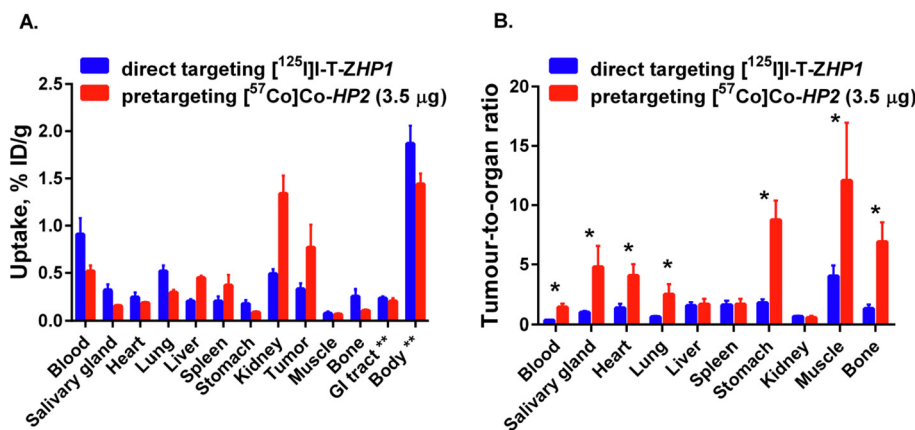


Fig. 11. (A) Comparison of direct targeting (black) 72 h after intravenous injection of $[^{125}\text{I}]\text{I-T-ZHP1}$ and pretargeting 24 h post $[^{57}\text{Co}]\text{Co-HP2}$ injection in BALB/C nu/nu mice bearing HER2-expressing SKOV-3 xenografts. (B) Comparison of tumor-to-organ uptake ratios for $[^{125}\text{I}]\text{I-T-ZHP1}$ (black) and pretargeted $[^{57}\text{Co}]\text{Co-HP2}$ (white). Data is presented as an average value from four animals \pm standard deviation. Asterisks (*) indicates significant difference ($p < 0.05$ in paired student's t-test). **Uptake in gastrointestinal tract (GI tract) and remaining body is presented as %ID per whole sample.

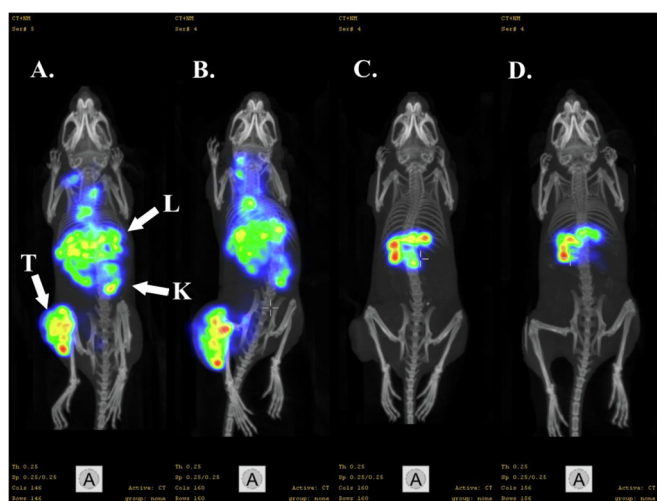


Fig. 12. SPECT imaging of BALB/C nu/nu mice bearing HER2-expressing SKOV-3 xenografts 24 h post $[^{57}\text{Co}]\text{Co-HP2}$ (2.7 MBq, 3.5 µg) injection. In (A) and (B) mice were pretargeted with 80 µg T-ZHP1 48 h prior to the injection of $[^{57}\text{Co}]\text{Co-HP2}$. In (C) and (D) mice were only injected with $[^{57}\text{Co}]\text{Co-HP2}$ i.e. without pretargeting. (T) Tumor, (K) Kidney, (L) Liver.

efforts to optimize our mAb-based PNA-mediated pretargeting should be harmonized with the development of a clearing agent. Finally, the method is versatile and may be extended to other applications. For example, it could be employed for beta cell imaging to measure the islet cell mass in the pancreas or following islet transplantation [54]. It may also be applied to accurately localize infectious and inflammatory foci throughout the body in patients suffering from chronic infectious or inflammatory diseases [16,55].

Conflict of interest statement

Vladimir Tolmachev and Anna Orlova are members of the Technical Advisory Board of Affibody AB, Stockholm.

Data availability statement

The raw/processed data required to reproduce these findings cannot be shared at this time due to technical or time limitations.

Supplementary data for this article is available as a Data in Brief communication [36].

Acknowledgments

This research was financially supported by grants from the Swedish Cancer Society [grant numbers CAN2018/436 (VT), CAN2014-474, CAN 2017/425 (AO)], the Swedish Research Council [grant numbers 2015-02353 (VT), 2015-02509 (AO), 2016-05207 (AEK)], the ProNova VINN Excellence Centre for Protein Technology [grant number 2015-04037 (AEK, KW)], the Swedish Agency for Innovation, VINNOVA [grant number 2016/04060 (AO)] and the Swedish Society for Medical Research (MA). No other potential conflict of interest relevant to this article is reported.

References

- [1] T.M. Behr, Trastuzumab and breast cancer, *N. Engl. J. Med.* 27 (2001) 995–996.
- [2] P.J. Perik, M.N. Lub-De Hooge, J.A. Gietema, W.T.A. Van Der Graaf, M.A. De Korte, S. Jonkman, J.G.W. Kosterink, D.J. Van Veldhuisen, D.T. Sleijfer, P.L. Jager, E.G.E. De Vries, Indium-111-labeled trastuzumab scintigraphy in patients with human epidermal growth factor receptor 2-positive metastatic breast cancer, *J. Clin. Oncol.* 24 (2006) 2276–2282, <https://doi.org/10.1200/JCO.2005.03.8448>.
- [3] E.C. Dijkers, T.H. Oude Munnink, J.G. Kosterink, A.H. Brouwers, P.L. Jager, J.R. De Jong, G.A. Van Dongen, C.P. Schröder, M.N. Lub-De Hooge, E.G. De Vries, Biodistribution of 89 Zr-trastuzumab and PET imaging of HER2-positive lesions in patients with metastatic breast cancer, *Clin. Pharmacol. Ther.* 87 (2010) 586–592,

- <https://doi.org/10.1038/clpt.2010.12>.
- [4] M. Altai, A. Orlova, V. Tolmachev, Radiolabeled probes targeting Tyrosine-Kinase receptors for personalized medicine, *Curr. Pharmaceut. Des.* 20 (2014) 2275–2292.
 - [5] A.C. Freise, A.M. Wu, In vivo imaging with antibodies and engineered fragments, *Mol. Immunol.* 67 (2015) 142–152, <https://doi.org/10.1016/j.molimm.2015.04.001>.
 - [6] A. Krasniqi, N. Devoogdt, F.Y. Frejd, M. Keyaerts, V. Tolmachev, I.V. Cellular, N. Medicine, M.I. Centre, Same-day imaging using small proteins : clinical experience and translational prospects in oncology, *J. Nucl. Med.* 59 (2018) 1–29, <https://doi.org/10.2967/jnumed.117.199901>.
 - [7] D.J. Green, J.M. Pagel, A. Pantelias, N. Hedin, Y. Lin, D.S. Wilbur, A. Gopal, D.K. Hamlin, O.W. Press, Pretargeted radioimmunotherapy for B-cell lymphomas, *Clin. Cancer Res.* (2007) 5598–5604, <https://doi.org/10.1158/1078-0432.CCR-07-1223>.
 - [8] S. Lindegren, S.H. Frost, Pretargeted radioimmunotherapy with α -particle emitting radionuclides, *Curr. Radiopharm.* 4 (2011) 248–260.
 - [9] M. Patra, K. Zarschler, H.J. Pietzsch, H. Stephan, G. Gasser, New insights into the pretargeting approach to image and treat tumours, *Chem. Soc. Rev.* 45 (2016) 6415–6431, <https://doi.org/10.1039/c5cs00784d>.
 - [10] M. Altai, R. Membreno, B. Cook, V. Tolmachev, B.M. Zeglis, Pretargeted imaging and therapy, *J. Nucl. Med.* 58 (2017) 1553–1559, <https://doi.org/10.2967/jnumed.117.189944>.
 - [11] C. Bailly, C. Bodet-Milin, C. Rousseau, A. Faivre-Chauvet, F. Kraeber-Bodéré, J. Barbet, Pretargeting for imaging and therapy in oncological nuclear medicine, *EJNMMI Radiopharm. Chem.* 2 (2017) 6, <https://doi.org/10.1186/s41181-017-0026-8>.
 - [12] P.E. Nielsen, M. Egholm, O. Buchardt, Peptide nucleic acid (PNA). A DNA mimic with a peptide backbone, *Bioconjug. Chem.* 5 (1994) 3–7, <https://doi.org/10.1021/bc00025a001>.
 - [13] G. Liu, K. Mang'era, N. Liu, S. Gupta, M. Rusckowski, D.J. Hnatowich, Tumor pretargeting in mice using $(99m)Tc$ -labeled morpholino, a DNA analog, *J. Nucl. Med.* 43 (2002) 384–391.
 - [14] Y. Wang, F. Chang, Y. Zhang, N. Liu, G. Liu, S. Gupta, M. Rusckowski, D.J. Hnatowich, Pretargeting with amplification using polymeric peptide nucleic acid, *Bioconjug. Chem.* 12 (2001) 807–816, <https://doi.org/10.1021/bc0100307>.
 - [15] G. Liu, C. Liu, S. Zhang, J. HE, N. Liu, S. Gupta, M. Rusckowski, D.J. Hnatowich, Investigations of $99mTc$ morpholino pretargeting in mice, *Nucl. Med. Commun.* 24 (2003) 697–705, <https://doi.org/10.1097/00006231-200306000-00013>.
 - [16] M. Rusckowski, T. Qu, F. Chang, D.J. Hnatowich, Pretargeting using peptide nucleic acid, *Cancer* 80 (1997) 2699–2705.
 - [17] K. Westerlund, H. Honarvar, V. Tolmachev, A. Eriksson Karlström, Design, preparation, and characterization of PNA-based hybridization probes for affibody-molecule-mediated pretargeting, *Bioconjug. Chem.* 26 (2015) 1724–1736, <https://doi.org/10.1021/acs.bioconjugchem.5b00292>.
 - [18] A. Leonidova, C. Foerster, K. Zarschler, M. Schubert, H.J. Pietzsch, J. Steinbach, R. Bergmann, N. Metzler-Nolte, H. Stephan, G. Gasser, In vivo demonstration of an active tumor pretargeting approach with peptide nucleic acid bioconjugates as complementary system, *Chem. Sci.* 6 (2015) 5601–5616, <https://doi.org/10.1039/c5sc00951k>.
 - [19] H. Honarvar, K. Westerlund, M. Altai, M. Sandström, A. Orlova, V. Tolmachev, A.E. Karlström, Feasibility of affibody molecule-based PNA-mediated radionuclide pretargeting of malignant tumors, *Theranostics* 6 (2016) 93–103, <https://doi.org/10.7150/thno.12766>.
 - [20] M. Altai, K. Westerlund, J. Velletta, B. Mitran, H. Honarvar, A.E. Karlström, Evaluation of affibody molecule-based PNA-mediated radionuclide pretargeting: development of an optimized conjugation protocol and ^{177}Lu labeling, *Nucl. Med. Biol.* 54 (2017) 1–9, <https://doi.org/10.1016/j.nucmedbio.2017.07.003>.
 - [21] K. Westerlund, M. Altai, B. Mitran, M. Konijnenberg, M. Oroujeni, C. Atterby, M. de Jong, A. Orlova, J. Mattsson, P. Micke, A.E. Karlström, V. Tolmachev, Radionuclide therapy of HER2-expressing human xenografts using affibody-based peptide nucleic acid-mediated pretargeting: in vivo proof of principle, *J. Nucl. Med.* 59 (2018) 1092–1098, <https://doi.org/10.2967/jnumed.118.208348>.
 - [22] A. Upadhyay, N.M. Ponzio, V.N. Pandey, Immunological response to peptide nucleic acid and its peptide conjugate targeted to transactivation response (TAR) region of HIV-1 RNA genome, *Oligonucleotides* 18 (2008) 329–335, <https://doi.org/10.1089/oli.2008.0152>.
 - [23] L.C. Boffa, P. Menichini, C. Bolognesi, G. Cutrona, S. Roncella, G.L. Damonte, E. Millo, M.R. Mariani, S. Matis, D. Russo, P. Ciliutti, M. Ferrarini, Lack of mutagenicity and clastogenicity of PNAE μ -NLS targeted to a regulatory sequence of the translocated c-myc oncogene in Burkitt's lymphoma, *Mutat. Res. Genet. Toxicol. Environ. Mutagen* 628 (2007) 129–137, <https://doi.org/10.1016/j.mrgentox.2006.11.009>.
 - [24] G. Cutrona, L.C. Boffa, M.R. Mariani, S. Matis, G. Damonte, E. Millo, S. Roncella, M. Ferrarini, The peptide nucleic acid targeted to a regulatory sequence of the translocated c-myc oncogene in Burkitt's lymphoma lacks immunogenicity: follow-up characterization of PNAEmu-NLS, *Oligonucleotides* 17 (2007) 146–150, <https://doi.org/10.1089/oli.2007.9999>.
 - [25] G. Mardirossian, K. Lei, M. Rusckowski, F. Chang, T. Qu, M. Egholm, D.J. Hnatowich, In vivo hybridization of technetium- 99m -labeled peptide nucleic acid (PNA), *J. Nucl. Med.* 38 (1997) 907–913.
 - [26] M. Brinkley, A brief survey of methods for preparing protein conjugates with dyes, haptens and crosslinking reagents, *Bioconjug. Chem.* 3 (1992) 2–13, <https://doi.org/10.1021/bc00013a001>.
 - [27] P.R. Spycher, C.A. Amann, J.E. Wehrmüller, D.R. Hurwitz, O. Kreis, D. Messmer, A. Rittler, A. Küchler, A. Blanc, M. Béhé, P. Walde, R. Schibli, Dual, site-specific modification of antibodies by using solid-phase immobilized microbial transglutaminase, *Chembiochem* 18 (2017) 1923–1927, <https://doi.org/10.1002/cbic.201700188>.
 - [28] L. Wang, G. Amphlett, W.A. Blattler, J.M. Lambert, W. Zhang, Structural characterization of the maytansinoid-monoclonal antibody immunconjugate, huN901-DM1, by mass spectrometry, *Protein Sci.* 14 (2005) 2436–2446.
 - [29] M. Abdollahpour-Alitappeh, M. Lotfinia, S. Razavi-Vakhshourpour, S. Jahandideh, H. Najminejad, K. Sineh Sepehr, R. Moazami, E. Shams, M. Habibi-Anbouhi, M. Abolhasani, Evaluation of factors influencing antibody reduction for development of antibody drug conjugates, *Iran. Biomed. J.* 21 (2017) 270–274.
 - [30] A. Konrad, A. Eriksson Karlström, S. Hober, Covalent immunoglobulin labeling through a photoactivable synthetic Z domain, *Bioconjug. Chem.* 22 (2011) 2395–2403, <https://doi.org/10.1021/bc200052h>.
 - [31] A. Perols, A.E. Karlström, Site-specific photoconjugation of antibodies using chemically synthesized IgG-binding domains, *Bioconjug. Chem.* 25 (2014) 481–488, <https://doi.org/10.1021/bc400440u>.
 - [32] A. Perols, M. Arcos Famme, A. Eriksson Karlström, Site-specific antibody labeling by covalent photoconjugation of Z domains functionalized for alkyne-azide cycloaddition reactions, *Chembiochem* 16 (2015) 2522–2529, <https://doi.org/10.1002/cbic.201500300>.
 - [33] L. Jendeberg, M. Tashiro, R. Tejero, B.A. Lyons, M. Uhlén, G.T. Montelione, B. Nilsson, The mechanism of binding staphylococcal protein A to immunoglobulin G does not involve helix unwinding, *Biochemistry* 35 (1996) 22–31, <https://doi.org/10.1021/bi9512814>.
 - [34] M. Tashiro, R. Tejero, D.E. Zimmerman, B. Celda, B. Nilsson, G.T. Montelione, High-resolution solution NMR structure of the Z domain of staphylococcal protein A, *J. Mol. Biol.* 272 (1997) 573–590, <https://doi.org/10.1006/jmbi.1997.1265>.
 - [35] F. Yu, P. Järver, P.Å. Nygren, Tailor-making a protein A-derived domain for efficient site-specific photocoupling to Fc of mouse IgG1, *PLoS One* 8 (2013), <https://doi.org/10.1371/journal.pone.0056597>.
 - [36] K. Westerlund, A. Vorobyeva, B. Mitran, A. Orlova, V. Tolmachev, A. Eriksson Karlström, M. Altai, Trastuzumab-based Peptide Nucleic Acids (PNA)-mediated Pretargeting: Data on PNA Synthesis, Affinity Determination and In Vivo Biodistribution, Data in Brief (2019) (submitted for publication).
 - [37] H. Wällberg, A. Orlova, Slow internalization of anti-HER2 synthetic affibody monomer 111In-DOTA-ZHER2:342-pep2: implications for development of labeled tracers, *Cancer Biother. Radiopharm.* 23 (2008) 435–442, <https://doi.org/10.1089/cbr.2008.0464>.
 - [38] V. Tolmachev, A. Orlova, K. Andersson, Human Monoclonal Antibodies, (2014), <https://doi.org/10.1007/978-1-62703-586-6>.
 - [39] J.Z. Hui, A. Al Zaki, Z. Cheng, V. Popik, H. Zhang, E.T. Luning Prak, A. Tsourkas, Facile method for the site-specific, covalent attachment of full-length IgG onto nanoparticles, *Small* 10 (2014) 3354–3363, <https://doi.org/10.1002/sml.201303629>.
 - [40] J.Z. Hui, A. Tsourkas, Optimization of photoactive protein Z for fast and efficient site-specific conjugation of native IgG, *Bioconjug. Chem.* 25 (2014) 1709–1719, <https://doi.org/10.1021/bc500305v>.
 - [41] J.R. Junutula, H. Raab, S. Clark, S. Bhakta, D.D. Leipold, S. Weir, Y. Chen, M. Simpson, S.P. Tsai, M.S. Dennis, Y. Lu, Y.G. Meng, C. Ng, J. Yang, C.C. Lee, E. Duenas, J. Gorrell, V. Katta, A. Kim, K. McDorman, K. Flagella, R. Venook, S. Ross, S.D. Spencer, W. Lee Wong, H.B. Lowman, R. Vandlen, M.X. Sliwkowski, R.H. Scheller, P. Polakis, W. Mallet, Site-specific conjugation of a cytotoxic drug to an antibody improves the therapeutic index, *Nat. Biotechnol.* 26 (2008) 925–932.
 - [42] R.R. Beerli, T. Hell, A.S. Merkel, U. Grawunder, Sortase enzyme-mediated generation of site-specifically conjugated antibody drug conjugates with high in vitro and in vivo potency, *PLoS One* 10 (2015) e0131177.
 - [43] S.L. Rice, C.A. Roney, P. Daumar, J.S. Lewis, The next generation of positron emission tomography radiopharmaceuticals in oncology, *Semin. Nucl. Med.* 41 (2011) 265–282, <https://doi.org/10.1053/j.semnuclmed.2011.02.002>.
 - [44] M.A. Deri, B.M. Zeglis, L.C. Francesconi, J.S. Lewis, PET imaging with ^{89}Zr : from radiochemistry to the clinic, *Nucl. Med. Biol.* 40 (2013) 3–14, <https://doi.org/10.1016/j.nucmedbio.2012.08.004>.
 - [45] J. Bostrom, L. Haber, P. Koenig, R.F. Kelley, G. Fuh, High affinity antigen recognition of the dual specific variants of Herceptin is entropy-driven in spite of structural plasticity, *PLoS One* 6 (2011) 1–12, <https://doi.org/10.1371/journal.pone.0017887>.
 - [46] E.W. Price, C. Orvig, Matching chelators to radiometals for radiopharmaceuticals, *Chem. Soc. Rev.* 43 (2014) 260–290, <https://doi.org/10.1039/c3cs60304k>.
 - [47] H. Björkelund, L. Gedda, M. Malmqvist, K. Andersson, Resolving the EGF-EGFR interaction characteristics through a multiple-temperature, multiple-inhibitor, real-time interaction analysis approach, *Mol. Clin. Oncol.* 1 (2013) 343–352, <https://doi.org/10.3892/mco.2012.37>.
 - [48] J.K. Kim, M. Firan, C.G. Radu, C.H. Kim, V. Ghetie, E.S. Ward, Mapping the site on human IgG for binding of the MHC class I-related receptor, FcRn., *Eur. J. Immunol.* 29 (1999) 2819–2825.
 - [49] C. Vaccaro, J. Zhou, R.J. Ober, E.S. Ward, Engineering the Fc region of immunoglobulin G to modulate in vivo antibody levels, *Nat. Biotechnol.* 23 (2005) 1283–1288, <https://doi.org/10.1038/nbt1143>.
 - [50] G. Liu, S. Dou, X. Chen, L. Chen, X. Liu, M. Rusckowski, D.J. Hnatowich, Adding a clearing agent to pretargeting does not lower the tumor accumulation of the effector as predicted, *Cancer Biother. Radiopharm.* 25 (2010) 757–762, <https://doi.org/10.1089/cbr.2010.0800>.
 - [51] R. Rossin, T. Lappchen, S.M. van den Bosch, R. Laforest, M.S. Robillard, Diels-alder reaction for tumor pretargeting: in vivo chemistry can boost tumor radiation dose compared with directly labeled antibody, *J. Nucl. Med.* 54 (2013) 1989–1995, <https://doi.org/10.2967/jnumed.113.123745>.
 - [52] M. Altai, A. Perols, M. Tsourma, B. Mitran, H. Honarvar, M. Robillard, R. Rossin,

- W. ten Hoeve, M. Lubberink, A. Orlova, A.E. Karlstrom, V. Tolmachev, Feasibility of affibody-based bioorthogonal chemistry-mediated radionuclide pretargeting, *J. Nucl. Med.* 57 (2016) 431–436, <https://doi.org/10.2967/jnumed.115.162248>.
- [53] J.H. Dam, B.B. Olsen, C. Baun, P.F. Høilund-Carlsen, H. Thisgaard, In vivo evaluation of a bombesin analogue labeled with Ga-68 and Co-55/57, *Mol. Imag. Biol.* 18 (2016) 368–376, <https://doi.org/10.1007/s11307-015-0911-z>.
- [54] G. Liu, S. Dou, A. Akalin, M. Rusckowski, P.R. Streeter, L.D. Shultz, D.L. Greiner, Pretargeting vs . direct targeting of human betalox5 islet cells subcutaneously implanted in mice using an anti-human islet cell antibody, *Nucl. Med. Biol.* 39 (2012) 645–651, <https://doi.org/10.1016/j.nucmedbio.2011.12.001>.
- [55] O.C. Boerman, J. Van Eerd, W.J.G. Oyen, F.H.M. Corstens, A 3-step pretargeting strategy to image infection, *J. Nucl. Med.* 42 (2001) 1405–1412.